

# Practical Electromechanical Design for Marine Systems

*Final Project Report*

郭亦寬 陳祈璋 劉柏均 范晨榆

# **Table of Contents**

## **1. Circular Tube Strain Measurement**

1. Objective
2. Experimental Method
3. Tube Fixation Method
4. Strain Gauge Placement
5. Strain Gauge Bonding
6. Applied External Forces
7. Strain Gauge Labeling
8. Test Results
9. Improved Experimental Results

## **2. Displacement Measurement**

1. Displacement Sensor Setup
2. Measurement Results
3. Error Analysis
4. Improved Experimental Results
5. Issues and Improvements
6. Process Demonstration

## **3. Visualization of Engineering Design Workflow**

1. COMSOL Operation Workflow
2. Automation of Computational Procedures
3. Predicted Displacement Using iFEM
4. Graphical Output

## **4. iFEM Program**

1. Simple Structure Validation
2. Complex Structure Validation

## **5. Presentation of iFEM Results**

1. Object Configuration
2. Physical Model Selection
3. Material Parameter Settings
4. Output Configuration
5. Automated Output Workflow
6. Deformation Results Visualization

# 1. Circular Tube Strain Measurement

## 1.1 Objective

Following the validation of strain gauge accuracy and experimental procedures in the previous semester, this study focuses on measuring the structural response of a circular tube representing a wind turbine tower.

Based on reference materials, strain values were measured at two structural elements of the circular tube. The experimental data were then compared with numerical simulation results obtained from ANSYS to verify measurement reliability.

In addition, the displacement of the circular tube under static external loading was measured and compared with numerical predictions generated using an inverse Finite Element Method (iFEM) program developed in MATLAB. This comparison was conducted to evaluate the accuracy of the structural health monitoring system in predicting the displacement behavior of wind turbine tower structures.

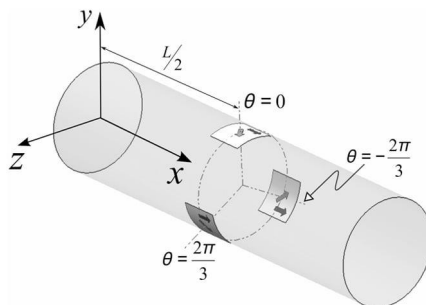


**Figure 1.** Schematic diagram of strain gauge placement.

## 1.2 Experimental Method

### Strain Measurement

To facilitate fixture installation, one end of the circular tube was manufactured as a cubic block to serve as the clamping interface, while the opposite end was used for suspending weights.

After securely fixing the tube with the clamp, strain gauges were positioned and bonded onto the tube according to the layout shown in Figure 1.

### **Displacement Measurement**

A displacement sensor was mounted at the free end of the circular tube to measure the magnitude of structural displacement.

The fully assembled experimental setup is shown in the figure below.



**Figure 2. Experimental Setup**

## **1.3 Circular Tube Fixation Method**

### **Problem 1**

Although the cubic block at the front end of the circular tube simplified the clamping process, the smooth metallic surfaces caused the fixture to slip easily, preventing the tube from being fully secured.

### **Problem 2**

When using the clamp, the edge of the cubic block needed to be aligned precisely with the edge of the fixture to avoid introducing additional support forces that could affect the experimental results. However, the uneven surface of the fixture made consistent alignment difficult, requiring further improvement to ensure accurate positioning during each installation.

### **Solution**

A U-shaped groove was fabricated using foam adhesive and wooden plates and placed between the clamp and the cubic block. This design increased friction to prevent slipping between the metal surfaces while also providing a flat reference plane for alignment. As a result, the circular tube could be mounted without unintended contact with the fixture, as shown in Figures 3 and 4.



**Figure 3.** Front view of the clamp and custom wooden fixture

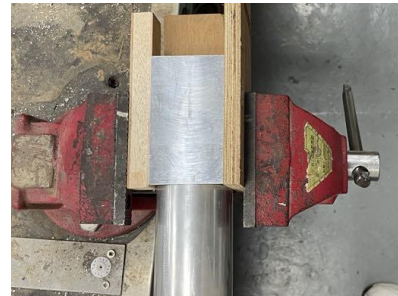


**Figure 4.** Top view of the clamp and custom wooden fixture

## 1.4 Strain Gauge Positioning

### Problem

As illustrated in Figure 1, the iFEM analysis required the circular tube to be divided into two elements. Strain gauges were placed at the center of each element with an angular spacing of **120°** around the circumference. Additionally, both longitudinal and oblique strain measurements were required at the same location.

### Solution

Three-axis strain gauges were utilized for installation and measurement, enabling simultaneous acquisition of longitudinal and oblique strain data at each measurement point.

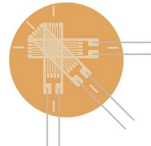


**Figure 5.** Schematic of the three-axis strain gauge

### Problem 2

As described in Problem 1, precise positioning of the two elements and the angular locations at  $0^\circ$ ,  $+120^\circ$ , and  $-120^\circ$  was required. Therefore, accurate spatial positioning became one of the primary challenges of this experiment.

### Solution

The center of the cubic block at the tube end was first defined as the  $0^\circ$  reference point. A measuring tape was then used to locate the quarter-length positions from both ends of the

circular tube, corresponding to the centers of the two elements.

Next, the circumference was calculated based on the tube diameter, and one-third of the circumference was used to determine the angular spacing. The measuring tape was wrapped around the tube to mark the 1/3 and 2/3 circumference positions, representing the +120° and -120° orientations.

Finally, a cross-alignment method was applied to complete the precise positioning of the strain gauges.



**Figure 6.** Locating the element centers using a measuring tape

## 1.5 Strain Gauge Bonding

After completing the cross-alignment procedure, the strain gauges were ready for installation. Based on the experimentally validated procedure from the previous semester, the bonding process began with surface preparation.

The outermost layer of the tube surface was first removed using coarse sandpaper. Fine sandpaper was then applied to smooth the surface and improve bonding quality. The center of the cross-aligned area was carefully cleaned, followed by wiping the surface with alcohol pads to eliminate contaminants.

To protect the circuitry, tape was applied starting from the lead wires to fully cover the front surface of the strain gauge. Adhesive was then applied to the prepared area, and the strain gauge was slowly pressed into place beginning from the wired end. Steady pressure was maintained for approximately 1–2 minutes to ensure proper adhesion.

Finally, the protective backing was peeled off slowly from the tail end at a 45° angle, completing the bonding process, as shown in Figure 6.

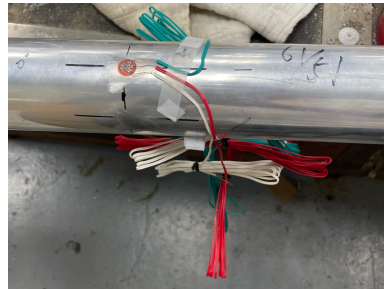


**Figure 7.** Completed strain gauge installation

## 1.6 External Forces

In this experiment, three levels of static external loads were applied: 1106 g (Weight 1), 2238.5 g (Weight 1 + Weight 2), and 3167 g (Weight 1 + Weight 2 + Weight 3).

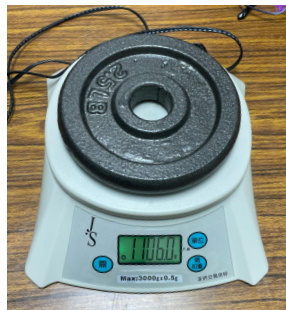


**Figure 8.** Weight 1



**Figure 9.** Weight 2



**Figure 10.** Weight 3

## 1.7 Strain Gauge Labeling

Due to the large number of strain gauges used in this experiment, a standardized labeling system was established to ensure consistency in experimental records and to prevent data entry errors. This labeling approach also facilitated post-experimental data processing. The numbering method is described as follows.

As shown in Figure 11, the element located closer to the fixed end was defined as Element 1, while the other was designated as Element 2. Additionally, as illustrated in Figure 12, the strain gauges positioned at  $-2\pi/3$  were assigned labels 1 and 2, after which the remaining gauges were numbered in a counterclockwise direction.

Odd-numbered gauges represent longitudinal strain measurements, whereas even-numbered gauges correspond to oblique strain measurements.



**Figure 11.** Element numbering schematic

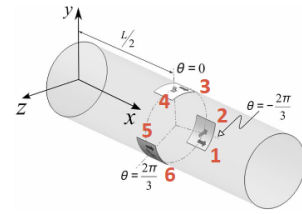


**Figure 12.** Strain gauge labeling schematic

## 1.8 Test Results

The following sections present the experimental results obtained under static external loads of 1106 g, 2238.5 g, and 3167 g.

Across all three loading conditions, the strain measurements exhibited a consistent trend: the overall strain observed in Element 1 was greater than that in Element 2. Furthermore, the relative distribution of strain at each measurement location remained consistent for both elements, with Position 3 showing the highest strain values.

**Table 1.** Average strain values under a 1106 g external load

應變 (ue)	1	2	3	4	5	6
element 1	-4.17	-1.21	9.80	3.37	-4.57	-1.65
element 2	-1.17	0.79	4.34	1.69	-0.84	0.22

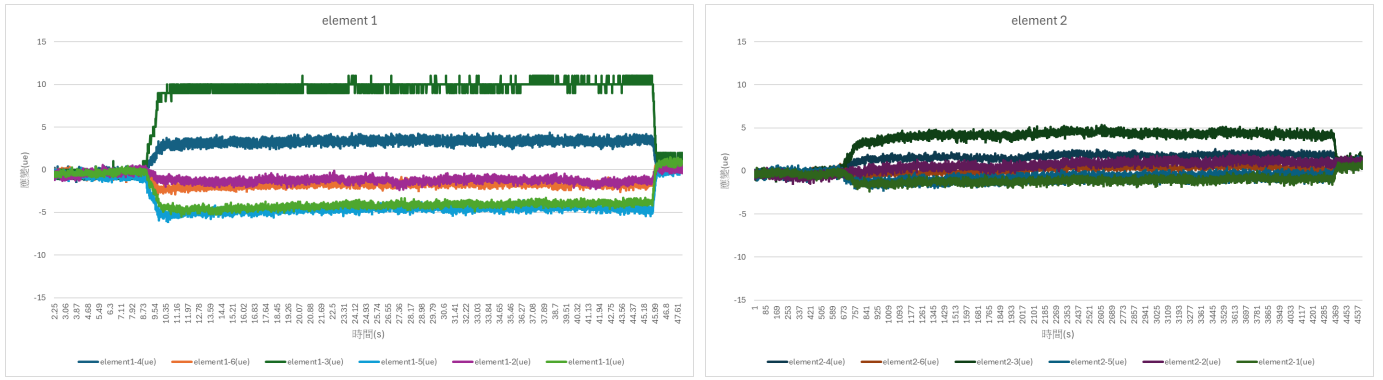


**Figure 13.** Strain–time relationship under a 1106 g external load

**Table 2.** Average strain values under a 2238.5 g external load

應變 (ue)	1	2	3	4	5	6
element 1	-10.62	-4.85	28.59	6.21	-10.31	-4.70
element 2	-2.81	2.08	6.99	1.92	-2.91	-1.22

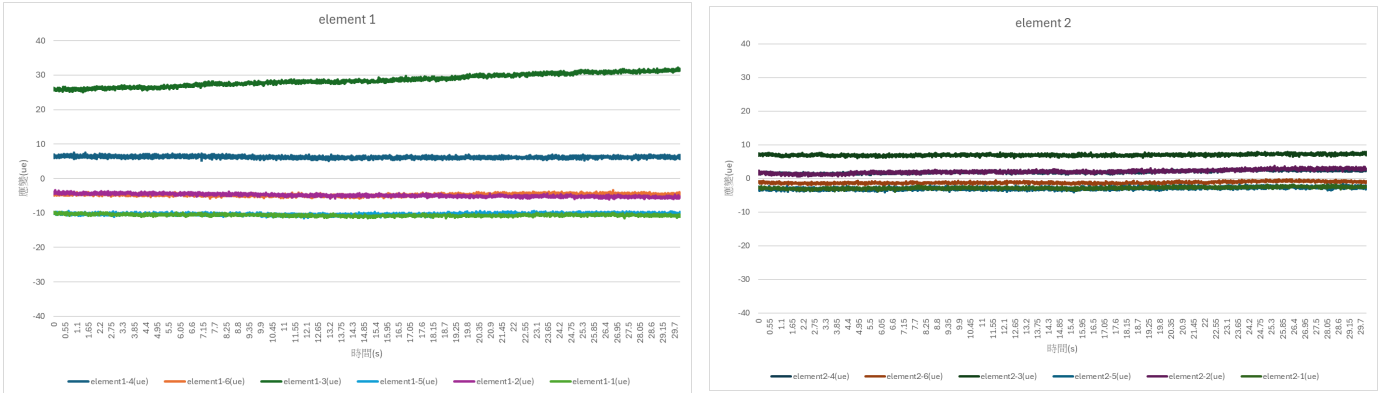


**Figure 14.** Strain–time relationship under a 2238.5 g external load

**Table 3.** Average strain values under a 3167 g external load

應變 (ue)	1	2	3	4	5	6
element 1	-13.96	-5.11	30.32	9.42	-13.92	-6.40
element 2	-3.88	1.32	9.65	3.44	-4.21	-1.85

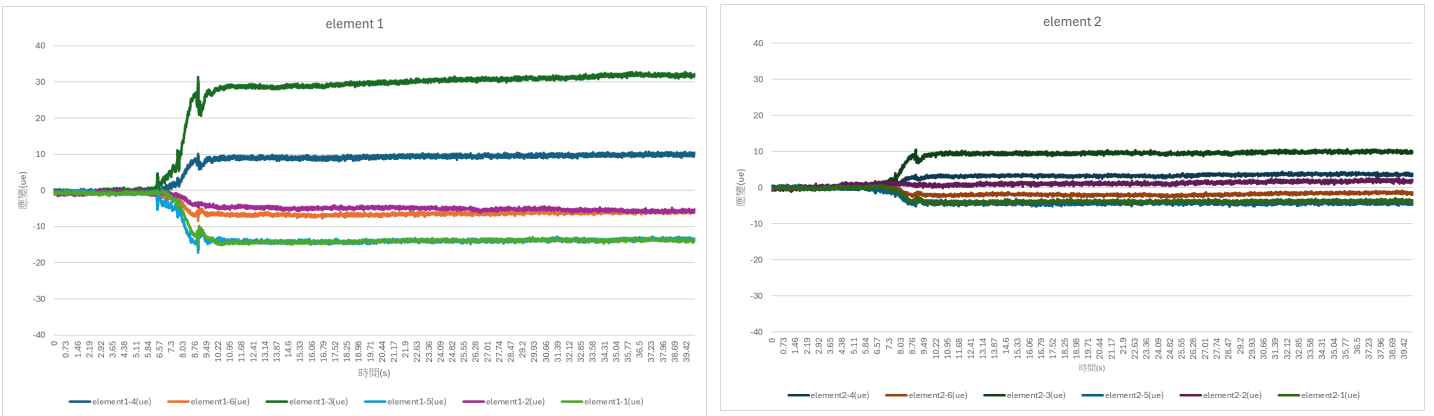


**Figure 15.** Strain–time relationship under a 3167 g external load

## 1.9 Improved Experimental Results

### Data Processing

During post-processing in Excel, significant fluctuations were observed in the strain measurements, causing the data series from different elements to overlap and reducing the readability of the plots, as shown in Figure 16. Therefore, an additional filtering step was performed to suppress oscillations and improve the clarity of data interpretation.

Since the purpose of filtering was solely to enhance visualization rather than alter the underlying measurements, a simple moving average filter was applied in Excel. Specifically, each data point was replaced with the average of its five neighboring points.

The filtered results are presented in Figure 17, where the fluctuations are noticeably reduced, resulting in improved plot readability.

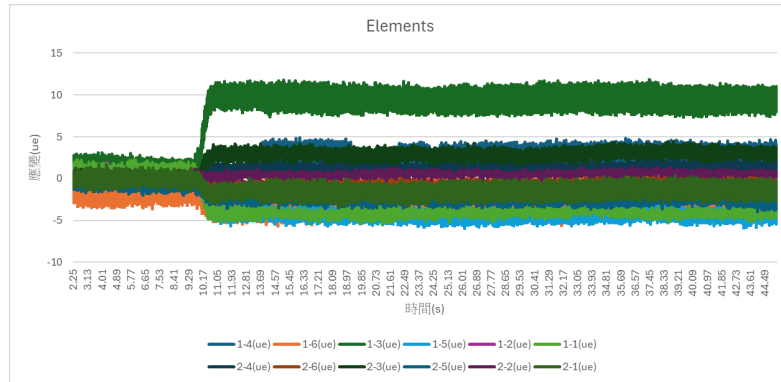


**Figure 16.** Original data plot

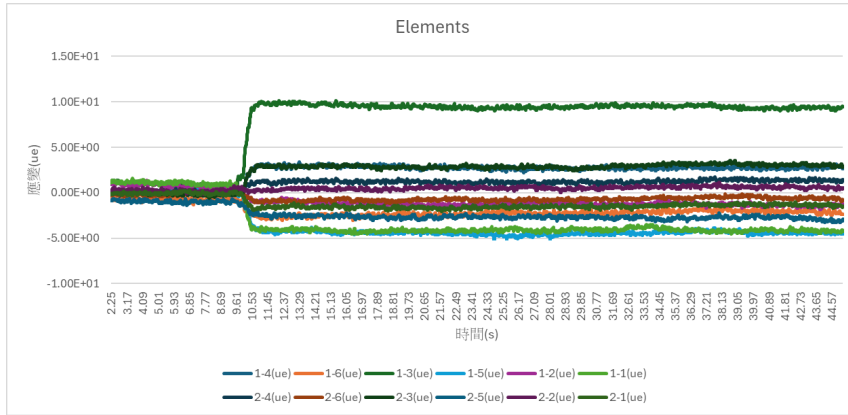


**Figure 17.** Filtered data plot

## Experimental Results

The following sections present the improved experimental results under static external loads of 1106 g, 2238.5 g, and 3167 g.

Across all three loading conditions, the strain measurements showed a consistent trend in which the overall strain in Element 1 was greater than that in Element 2. Additionally, the relative strain distribution at each measurement location was identical for both elements, with Position 3 exhibiting the highest strain values.

**Table 4.** Average strain values under a 1106 g external load

應變(ue)	1	2	3	4	5	6
element 1	-4.12	-1.25	9.47	2.77	-4.44	-2.22
element 2	-1.49	0.56	2.94	1.24	-2.71	-0.68

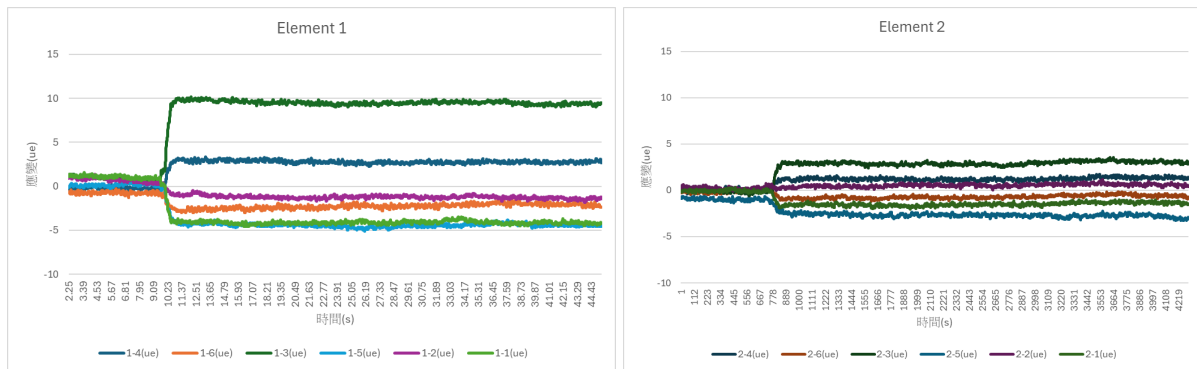


**Figure 18.** Strain–time relationship under a 1106 g external load

**Table 5.** Average strain values under a 2238.5 g external load

應變(ue)	1	2	3	4	5	6
element 1	-10.43	-4.62	27.83	6.33	-10.19	-4.59
element 2	-2.77	2.08	7.08	1.98	-2.88	-1.16

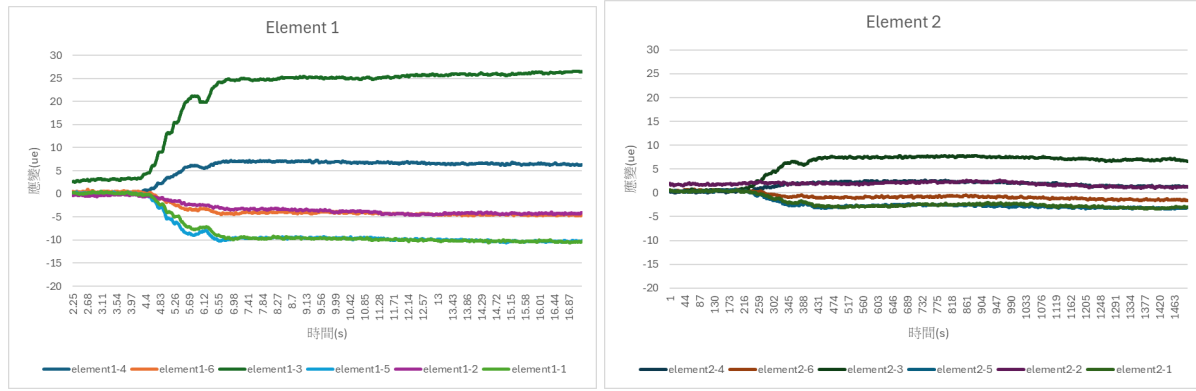


**Figure 19.** Strain–time relationship under a 2238.5 g external load

**Table 6.** Average strain values under a 3167 g external load

應變(ue)	1	2	3	4	5	6
element 1	-13.89	-5.23	30.65	9.52	-13.84	-6.30
element 2	-3.86	1.40	9.71	3.45	-4.18	-1.80

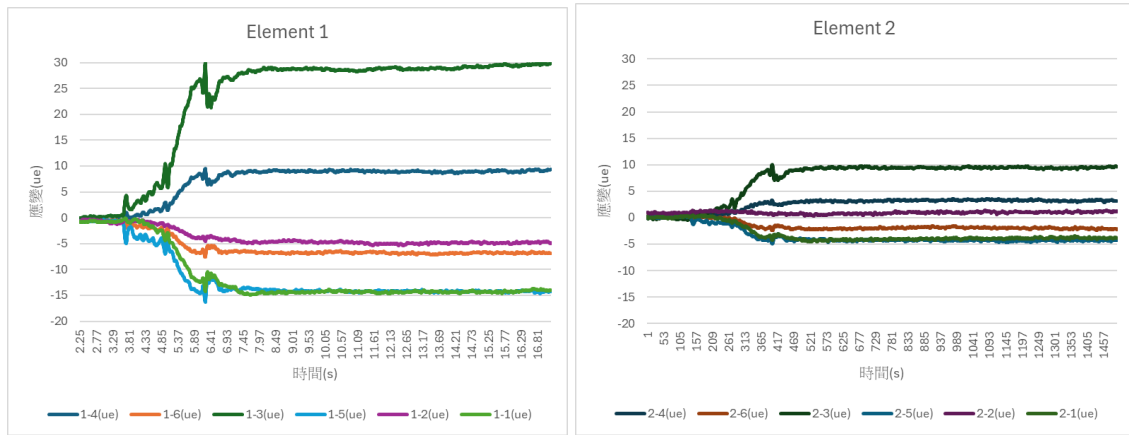


**Figure 20.** Strain–time relationship under a 3167 g external load

## 2. Displacement Measurement

### 2.1 Displacement Sensor Setup

#### Problem 1:

The displacement sensor needed to be positioned above the circular tube at the end where the weights were suspended. Therefore, the sensor had to be securely fixed in a vertical orientation directly above the tube, while the mounting method could not make contact with the tube.

#### Problem 2:

How to enable the displacement sensor to measure both tensile and compressive displacement.

#### Solution:

A tripod equipped with anti-slip pads was used to stabilize the setup, and the displacement sensor was fastened to the tripod using cable ties. The tripod height was adjusted so that the sensor could properly contact the top surface of the circular tube.

To allow measurement of both compression and tension, the sensor was pre-compressed to approximately half of its measurement range before being placed against the tube. The device was then zeroed prior to measurement, allowing compression and tension to be identified based on the positive and negative readings. The completed setup is shown in Figure 15.



**Figure 21.** Completed displacement sensor setup

### 2.2 Displacement Measurement Results

Table 7 and Figure 16 present the displacement measurement data. The results indicate that all measured displacements were less than 2 mm, and that displacement was proportional to the magnitude of the applied external load. These values will serve as validation data for the iFEM program, which will be discussed in a later section.

	1106g	2238.5g	3167g
位移(mm)	0.65	1.32	1.93

**Table 7. Displacement measurement results**

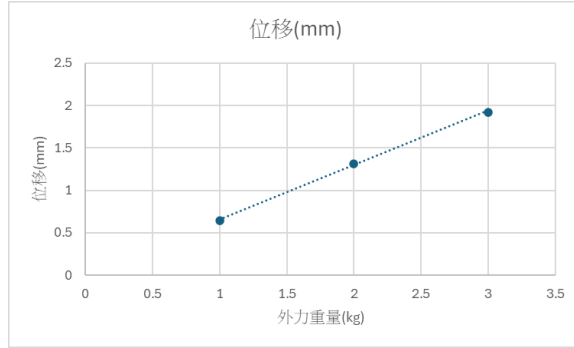


**Figure 22.** Relationship between applied load and displacement

### 2.3 Error Analysis

Several factors contributed to measurement error:

After prolonged experimentation, the clamp securing the circular tube became slightly loosened, causing the tube to tilt and resulting in inaccurate displacement measurements. To address this issue, ANSYS simulations were used for secondary validation. The error can be reduced by re-tightening the clamp after each experimental run.

Due to the complexity of the circuit configuration, particularly at the DAQ connections, wires may have come into contact with one another, potentially causing short circuits. This issue is typically identifiable through abnormally high strain readings. It can be resolved by organizing the wiring with protective sleeves or separating contact points using tweezers.

Additionally, the suspended weights may have contacted the tripod or induced oscillations. Selecting an appropriate suspension rope length helps mitigate this problem; excessively long ropes increase oscillation, while overly short ropes are more likely to contact the tripod. After implementing these adjustments, the measurement error was significantly reduced.

### 2.4 Improved Experimental Results

Table 8 and Figure 17 present the displacement data obtained after improvements to the experimental procedure. The measured displacement ranged approximately from 0.9 mm to 3.5 mm, and displacement remained proportional to the magnitude of the applied external load. These values will serve as validation data for the iFEM program, which will be discussed in a later section.

**Table 8.** Improved displacement measurement results

	1106g	2238.5g	3167g
毫米(mm)	0.952	2.337	3.521

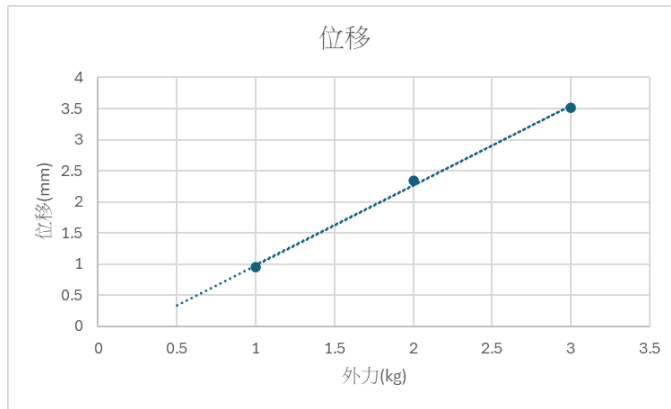


**Figure 23.** Relationship between applied load and displacement after experimental improvements

## 2.5 Issues and Improvements

### Stability of the Fixed End

During the experiment, displacement measurements taken at the fixed end revealed that the clamp loosened after several test runs, introducing errors into the data. To address this issue, an additional clamp was installed to secure the vertical direction, as shown in Figure 24. Furthermore, the clamp was re-tightened prior to each experiment to ensure the stability of the fixed end.

### Displacement Sensor Mounting Method

The displacement sensor mounting method was modified by replacing cable ties with screw-based fastening to the tripod, as shown in Figure 25. This adjustment improved the positional stability of the sensor.



**Figure 24.** Vertical clamp



**Figure 25.** Displacement sensor secured with screws

### Unit Conversion

After implementing the improvements described above, it was observed that although the experimental data showed significant deviation, the values differed from the expected results by a consistent scaling factor. This prompted further investigation into potential error sources beyond the experimental setup.

Following repeated validation using MATLAB and ANSYS, it was determined that the electrical signal from the displacement sensor had been converted into torque units in the computer output rather than the intended millimeters, resulting in the discrepancy. After entering the correct calculation parameters, the measurement error was reduced to a minimal level.

### Improvement of Displacement Measurement Error

To measure displacement in both positive and negative directions, the original method set the zero position of the displacement sensor at the midpoint of its range. However, experimental observations showed that setting the zero position at the lowest point significantly reduced measurement error. Furthermore, the greater the distance between the zero position and the bottom limit, the larger the resulting error became.

### Weight Selection

To improve measurement precision, calibrated weights were used, with the maximum load not exceeding 5 kg. However, due to the inherent strength of the metal cylindrical structure, an external load of approximately 4 kg produced only millimeter-level displacement. Given that the displacement sensor has a measurement range of up to 100 cm, increasing the applied load would produce more noticeable deformation in the cylinder. Expanding the displacement toward the centimeter scale would help reduce relative measurement error.

## Leveling

Another potential source of error was improper leveling. Although the displacement sensor was firmly secured to the tripod after iterative improvements, its alignment and levelness had not yet been verified. A non-level sensor may measure diagonal displacement rather than true longitudinal displacement, leading to inaccurate results.

In future work, a small spirit level can be placed on the sensor surface to confirm proper leveling. Similarly, a level can be used at the clamping location of the cylinder to ensure it is horizontally aligned. Verifying both conditions ensures that the displacement sensor is properly positioned at a zero-degree orientation.

## 2.6 Process Demonstration



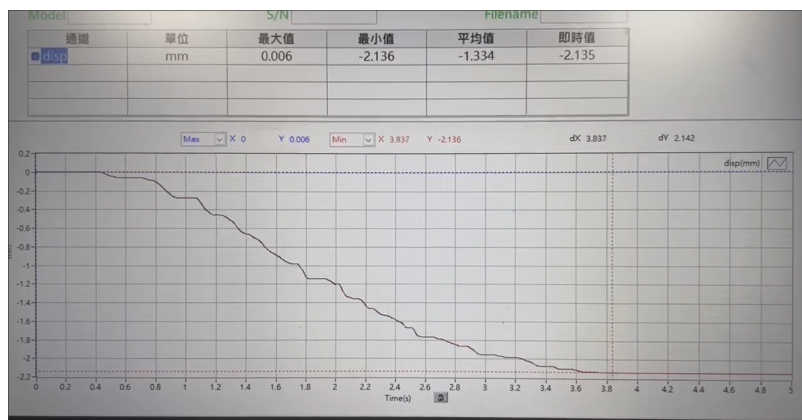
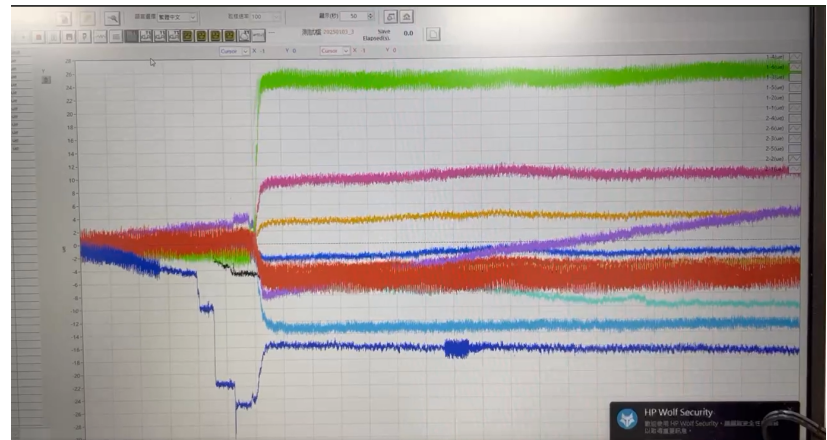
Zero the measurement software (displacement and strain), begin data recording, and start the measurement.

Slowly suspend the weights to avoid oscillation and prevent contact with the tripod.



Wait until the weights stabilize and the rope stops oscillating, then begin recording the results.

Observe the strain measurements to ensure there are no unreasonable extreme values.



Observe the displacement measurements to confirm they are within the millimeter range, verify the absence of extreme values, and compare the results with MATLAB and ANSYS.

### 3. Visualization of the Engineering Design Workflow

#### 3.1 COMSOL Operation Workflow

##### 3D Model

The 3D model serves as the foundation of COMSOL simulations and is used to describe the geometric structure of the object under study. In COMSOL, users can create basic shapes using built-in geometry tools or import CAD files to incorporate more complex structures.

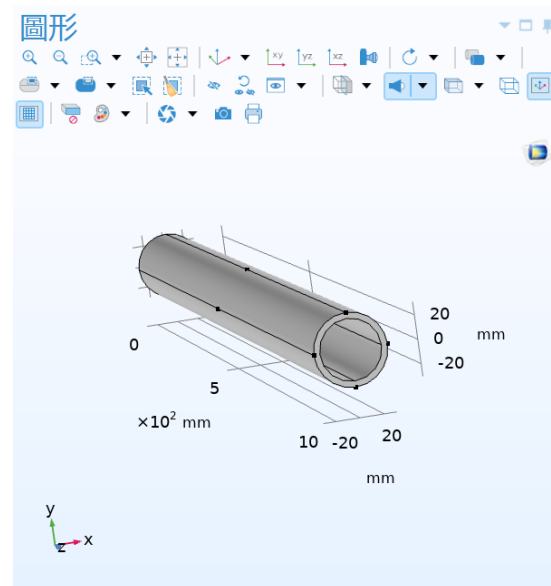


**Figure 17.** Creating a 3D model

##### Physics Setup

The physics setup involves defining the physical fields and boundary conditions of the problem. COMSOL provides a wide range of physics interfaces, such as structural mechanics, heat transfer, fluid dynamics, and electromagnetics, allowing users to select the appropriate module based on simulation requirements.



**Figure 18.** Solid Mechanics physics setup in COMSOL

## Mesh Setup

Mesh configuration is critical in numerical simulations, as it directly affects computational accuracy and efficiency. In COMSOL, meshes can be generated automatically or manually refined, and multiple element types are supported, including tetrahedral and hexahedral meshes.

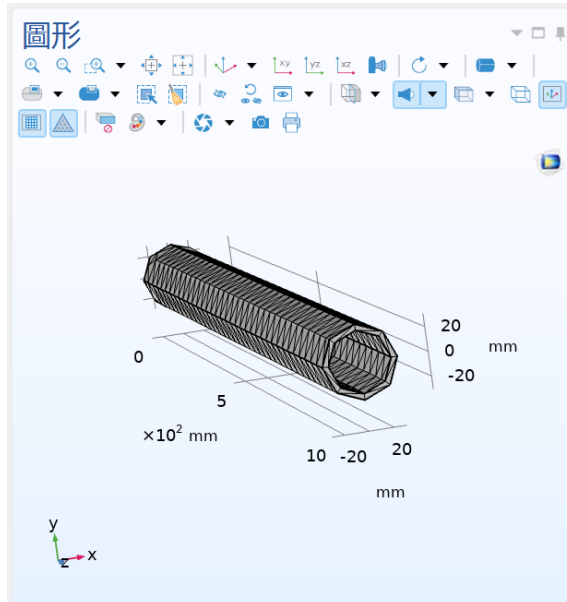


**Figure 19.** Mesh setup

## Solver Setup

Analysis configuration includes selecting the solver, defining time steps, and specifying

convergence criteria. COMSOL provides both stationary and transient analysis options and automatically configures an appropriate solver based on the selected physics interface.

For multiphysics coupling problems, it is necessary to properly define the solution sequence and coupling strategy between different physical fields. Additionally, correct initial and boundary conditions must be ensured to prevent convergence issues.

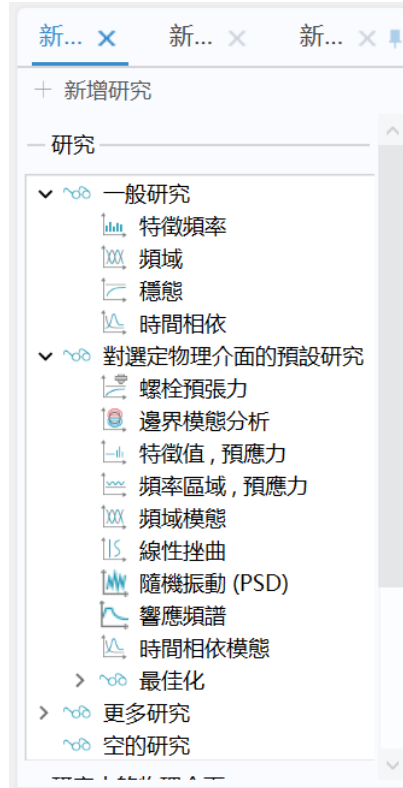


**Figure 20.** COMSOL solver setup

### Result Output and Post-Processing

After the simulation is completed, COMSOL provides various post-processing tools for result visualization and data analysis. Users can generate spatial distribution plots of physical quantities to better understand the behavior of the physical fields. The software also supports extracting data from specific locations and exporting it for use as a real-time system analysis tool.

## 3.2 Automation of Computational Procedures

The ultimate objective of this experiment is to integrate the inverse Finite Element Method (iFEM) model with COMSOL simulations to achieve a Digital Twin that combines numerical computation with a physical model. After the iFEM model completes its calculations, the predicted displacement values are dynamically transmitted to the COMSOL simulation environment to generate corresponding result visualizations. To ensure the efficiency and

practicality of the digital twin system, the entire operational workflow must be highly automated.

This process automatically inputs displacement values at specified locations while keeping other parameters unchanged. Based on the input data, the system updates the boundary conditions or displacement parameters within the COMSOL model and initiates the simulation. Upon completion, result images are automatically generated and saved in a predefined format. These images are stored in a designated folder according to experimental requirements, enabling subsequent processes to directly access the files for visualization or further analysis. This establishes a complete, streamlined, and repeatable digital twin workflow.

The automation of this process significantly reduces manual operation time and the likelihood of human error while improving overall experimental efficiency and reproducibility. Furthermore, seamless integration with the iFEM model allows for more flexible parameter adjustments and result analysis, providing a solid technical foundation for future multiphysics simulations and control system design.

### **3.3 Displacement Input Using iFEM Predictions**

Precomputing nodal displacements using the inverse Finite Element Method (iFEM) and applying these values as known conditions for subsequent Finite Element Method (FEM) analysis is an effective numerical strategy. FEM can then be used to estimate additional physical quantities within the structure, such as stress, strain, or temperature distribution. The primary advantage of this approach lies in the ability of inverse analysis to rapidly identify displacement information at critical nodes, thereby reducing the computational scope and precision requirements of the subsequent FEM analysis.

Within this workflow, FEM calculations can employ a relatively coarse mesh for discretization because the nodal displacements already provide baseline boundary conditions. This eliminates the need for high-precision simulation across all structural details. The use of a coarse mesh significantly shortens computation time and reduces hardware demands, including memory usage and processor performance, thereby improving overall computational efficiency and real-time capability.

For example, regions exhibiting non-uniform physical distributions or rapid variation can be modeled with moderate mesh density, while areas with smaller strain gradients or more uniform distributions can be approximated using a coarser mesh. This mesh optimization strategy substantially lowers computational cost while maintaining result accuracy.

Additionally, since iFEM provides high-precision nodal displacement data in advance, these values can be directly applied as boundary conditions and initial parameters in FEM analysis. This further reduces the solution space and avoids unnecessary iterative computations. The

staged computation approach also enables parallel processing across multiple devices, such as executing iFEM and FEM on separate computational nodes to further enhance overall efficiency.

In practical engineering applications, this approach is particularly suitable for real-time monitoring and dynamic analysis. For example, in Structural Health Monitoring (SHM), iFEM can be used to rapidly capture displacement variations at critical nodes, after which FEM can estimate the stress and strain distributions throughout the structure. This workflow not only improves analytical efficiency but also meets real-time requirements while maintaining result accuracy, providing a basis for rapid fault warnings and maintenance decision-making.

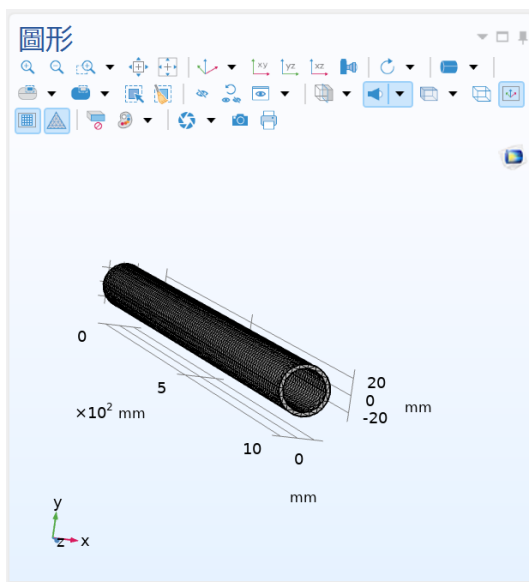


**Figure 21.** Mesh configuration in the Finite Element Method

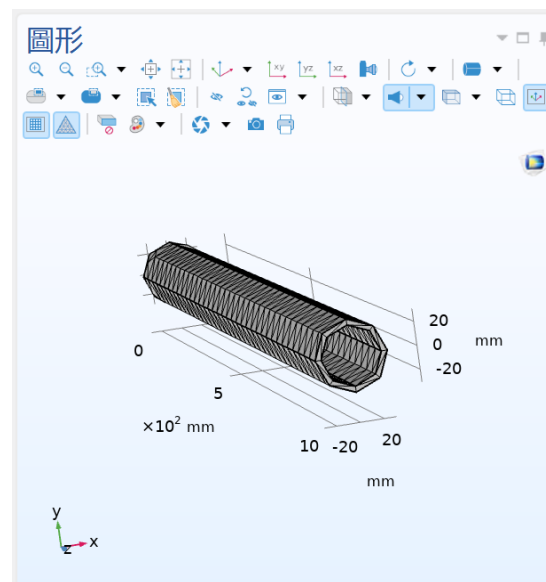


**Figure 22.** Mesh configuration after applying known nodal displacements

### 3.4 Image Output

#### Displacement Visualization

After the computation is completed, the exported images use displacement as the primary feature for color mapping. This visualization method intuitively presents the distribution of displacement across different locations. By converting displacement values into color gradients, distinct colors represent varying magnitudes of displacement, allowing rapid identification of structural deformation.

The advantage of this approach lies in its clarity, enabling quick detection of regions with excessive displacement or abnormal deformation, thereby facilitating the identification of potential structural issues. For example, in structural health monitoring, displacement contour plots allow engineers to rapidly locate areas that may contain cracks, fractures, or excessive deformation and take appropriate maintenance or reinforcement actions. This not only improves inspection efficiency but also helps detect hidden structural defects at an early stage, reducing the risk of catastrophic failure while making the structural condition easier to understand for non-specialists.

More importantly, combining the rapid visual judgment of human observers with machine-based detection significantly enhances overall inspection effectiveness. Automated analysis provides precise and consistent data, while human interpretation supports fast pattern recognition and anomaly detection. This human–machine collaboration improves diagnostic accuracy, reduces the risk of misinterpretation, and ensures the reliability of inspection results.

In practical applications, this visualization technique can also be integrated with augmented reality (AR) and virtual reality (VR) technologies to provide a more immersive and interactive inspection experience. For instance, engineers could use AR glasses to view real-time displacement distributions during field inspections, improving both operational efficiency and accuracy.

In summary, color-mapped displacement visualization is an intuitive and efficient method for structural assessment. It enables rapid identification of abnormal deformation and, through human–machine collaboration, significantly enhances inspection accuracy and efficiency. When combined with advanced imaging techniques and intelligent analysis tools, this method demonstrates strong potential for future applications in structural health monitoring, smart city development, and real-time management of engineering systems.

## **Strain Visualization**

The visualization of strain values follows a similar principle to displacement visualization, aiming to present the strain distribution throughout the structure. By expressing strain magnitudes as color gradients, observers can clearly identify variation trends and regions of strain concentration. This graphical representation is highly valuable for rapidly assessing structural health and potential failure risks.

Typically, Finite Element Method (FEM) results provide the distribution of the strain field rather than critical fracture strain values directly associated with material properties. Therefore, material parameters such as yield strain or critical fracture strain are usually determined in advance through material testing and then analyzed alongside FEM simulation results. Visualizing strain data allows for rapid evaluation of whether the structure has reached the threshold for plastic deformation or is at risk of localized fracture.

If the strain map indicates that a region exceeds the material's yield strength, it can be reasonably inferred that the area has entered the plastic deformation stage and may be at risk

of permanent structural damage or failure. Similarly, strain values approaching or surpassing the critical fracture threshold may signal an imminent or existing structural break. Through this visualization-based assessment, engineers can quickly locate the most vulnerable regions of a structure and reinforce or repair these critical areas to prevent potential hazards.

## 4. iFEM Program Validation

### 4.1 Simple Structure Validation

The three-dimensional iFEM program has been successfully validated. The validation results are presented below.

Schematic diagram of the validation structure geometry:

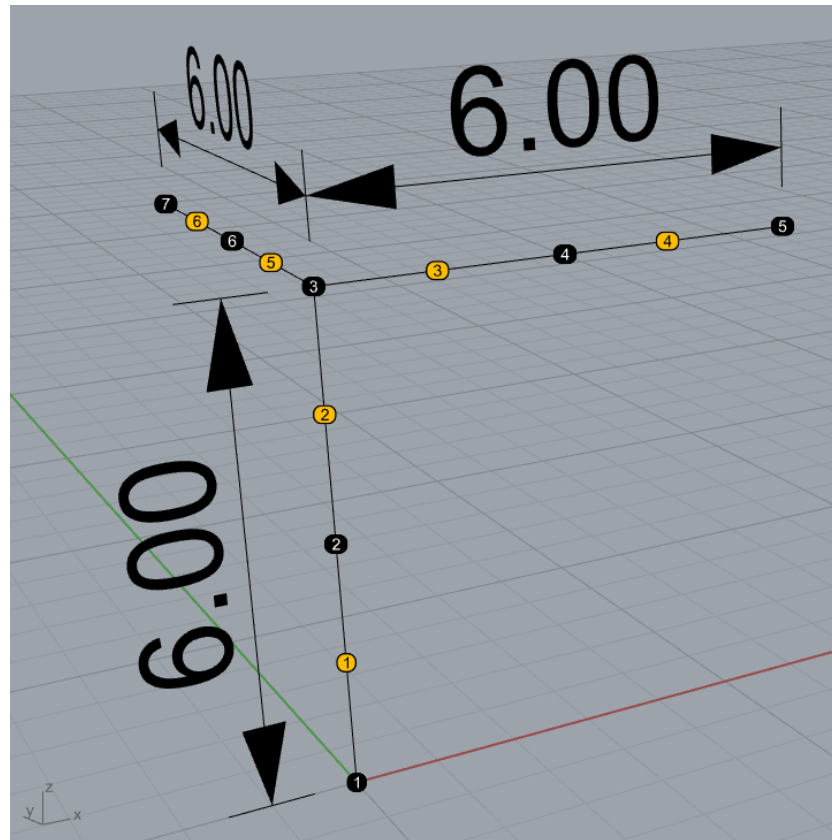


**Figure 23.** Structural schematic

The black annotated points represent node numbers, while the yellow annotations indicate element numbers. Each element has a length of 3 meters and a circular cross-section with a radius of 0.1 meters.

#### Local Coordinate System Settings:

Elements 1 and 2: local-x: (0,0,1), local-y: (1,0,0), local-z: (0,1,0)

Elements 3 and 4: local-x: (1,0,0), local-y: (0,1,0), local-z: (0,0,1)

Elements 5 and 6: local-x: (0,1,0), local-y: (1,0,0), local-z: (0,0,-1)

**External Force and Boundary Conditions:**

Node 1 is fixed.

Node 5 is subjected to an external force of 100 N in the y-direction.

Node 7 is subjected to an external force of -50 N in the z-direction.

位移結果：

Displacement in the x-direction

Node	1	2	3	4	5	6	7
Comsol	0.00000E+00	4.29720E-05	1.71890E-04	1.71890E-04	1.71890E-04	-7.15050E-04	-1.60200E-03
Matlab	0.00000E+00	4.29718E-05	1.71887E-04	1.71887E-04	1.71887E-04	-7.21927E-04	-1.61574E-03
error(%)		0.000385	0.001548	0.001548	0.001548	0.961726	0.857739

Displacement in the y-direction:

Node	1	2	3	4	5	6	7
Comsol	0.00000E+00	2.29180E-04	8.02140E-04	1.83230E-03	3.03440E-03	8.02140E-04	8.02140E-04
Matlab		2.29323E-04	8.02421E-04	1.83961E-03	3.04870E-03	8.02421E-04	8.02421E-04
error(%)		0.062429	0.035009	0.399192	0.471108	0.035009	0.035009

Displacement in the z-direction:

Node	1	2	3	4	5	6	7
Comsol	0.00000E+00	-4.77460E-08	-9.54930E-08	-2.00630E-04	-4.15490E-04	-7.59260E-04	-1.60440E-03
Matlab	0.00000E+00	-4.77465E-08	-9.54930E-08	-2.00701E-04	-4.15560E-04	-7.59335E-04	-1.60452E-03
error(%)		0.001011	0.000036	0.035239	0.016817	0.009819	0.007310

**Table 9.** Displacements and errors in three directions for the simple structure

The maximum error is only 0.96%, therefore the validation is considered successful. The next step is to proceed with validation on a more complex structure.

## 4.2 Complex Structure Validation

Schematic diagram of the validation structure:

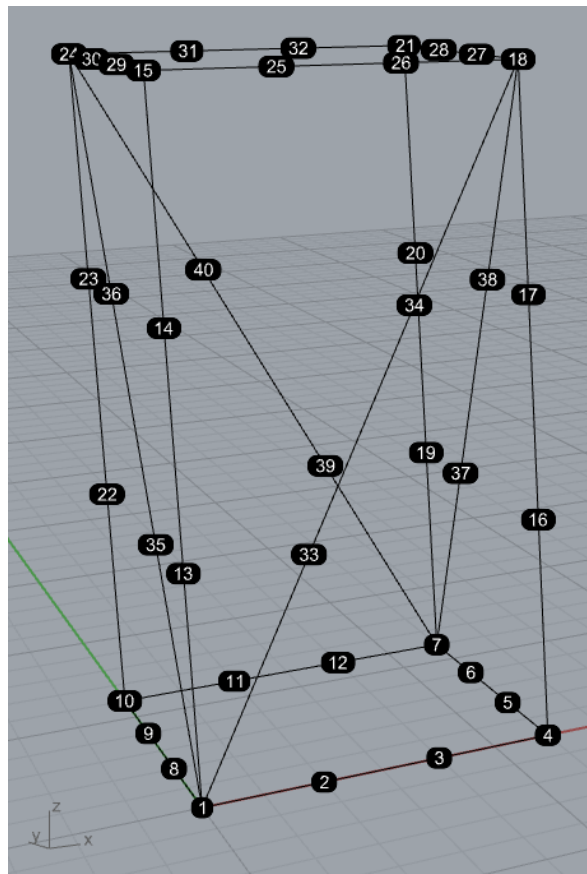


**Figure 24.** Node numbering diagram

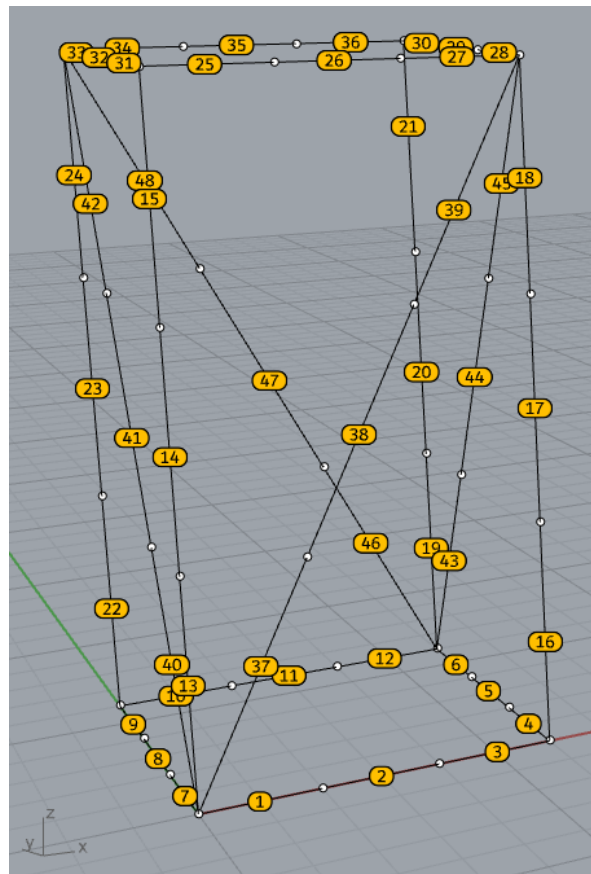


**Figure 25.** Element numbering diagram

The structure has a circular cross-section with a radius of 0.2 m. Its length and width are 6 m, and its height is 12 m.

### External Force and Boundary Conditions:

Nodes 1, 4, 7, and 10 are fixed.

Nodes 18 and 21 are subjected to an external force of 100,000 N in the x-direction.

## Results

The following figures were generated in MATLAB after computation and are compared with the COMSOL results.

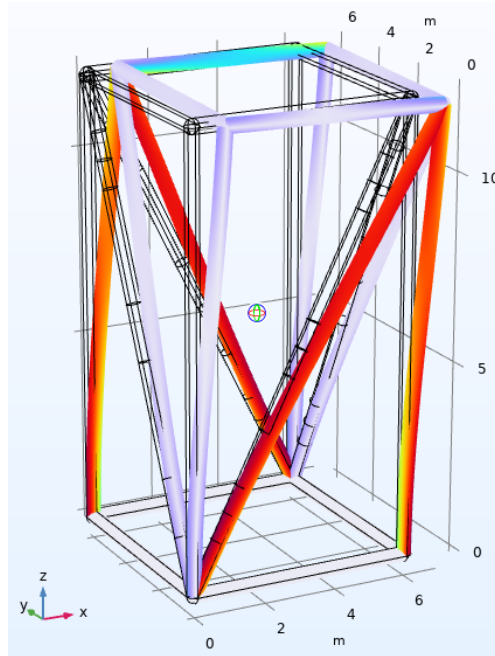


**Figure 26.** COMSOL displacement

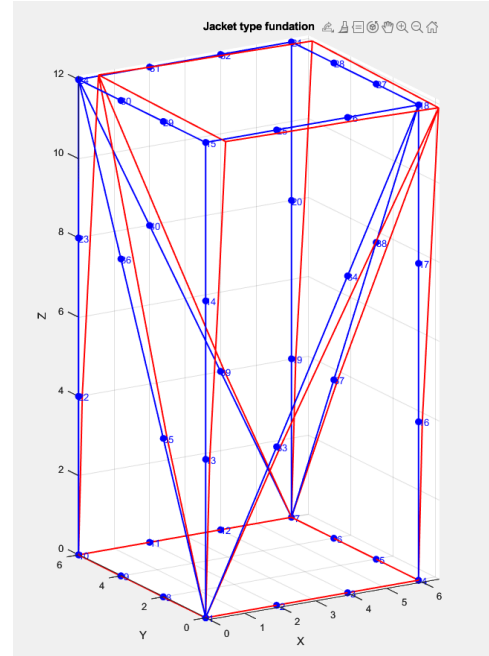


**Figure 27.** MATLAB displacement

### Displacement Error

Since the structure contains 40 nodes, there are 120 displacement data points in total (40 nodes  $\times$  3 directions), which cannot all be presented. Therefore, the comparison focuses on Nodes 18 and 21, where the displacement is the largest.

**Node 18**

	x	y	z
COMSOL	4.52128E-04	-1.87960E-04	-9.44350E-05
Matlab	4.52559E-04	-1.87968E-04	-9.44366E-05
error(%)	0.095302827	0.004154558	0.001655549

**Table 10.** Displacement and error at Node 18

**Node 21**

	x	y	z
COMSOL	4.74E-04	-1.88E-04	-4.53E-07
Matlab	4.68E-04	-1.88E-04	-4.52E-07
error(%)	1.309309608	0.001623988	0.328986446

**Table 11.** Displacement and error at Node 21

## 5. Presentation of iFEM Calculation Results

### 5.1 Object Configuration

To generate visualized results, COMSOL was used as an auxiliary software tool for graphical output. First, a 3D model of the test object was manually created. The model was developed using SolidWorks for three-dimensional design, exported as a file, and then imported into COMSOL.

The specifications of the circular tube are listed in Table 12.

length(mm)	Outer diameter (mm)	Inner diameter (mm)
1000	61	51

**Table 12.** Circular tube specifications

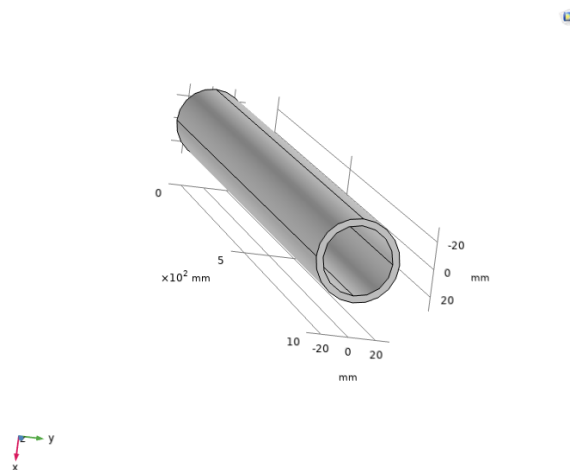


**Figure 28.** 3D model of the circular tube

### 5.2 Physics Model Selection

Since structural deformation in the experiment is caused by external force boundaries and fixed constraints, the physics model only requires the selection of Solid Mechanics. The fixed boundaries, external forces, and prescribed deformation are then defined accordingly.

### 5.3 Material Parameter Settings

The experimental cylinder is made of 6061 aluminum alloy. Its material parameters are listed in Table 13.

密度(kg/m <sup>3</sup> )	Poisson ratio(1)	Youngs' Modulus(GPa)
2700	0.33	69.9

**Table 13.** Material parameters

## 5.4 Output Settings

To make the deformation magnitude of the cylinder easier to identify visually, the deformation was scaled by a factor of 25, and color distribution was used to represent displacement at each location.

## 5.5 Automated Output Workflow

The data computed by iFEM were first preprocessed and then incorporated into a MATLAB program, where the prescribed displacement values were updated for further computation. After configuring the output image specifications, the generated images were saved to a predefined folder. Finally, Python was used to compile the images from the folder into a video file.

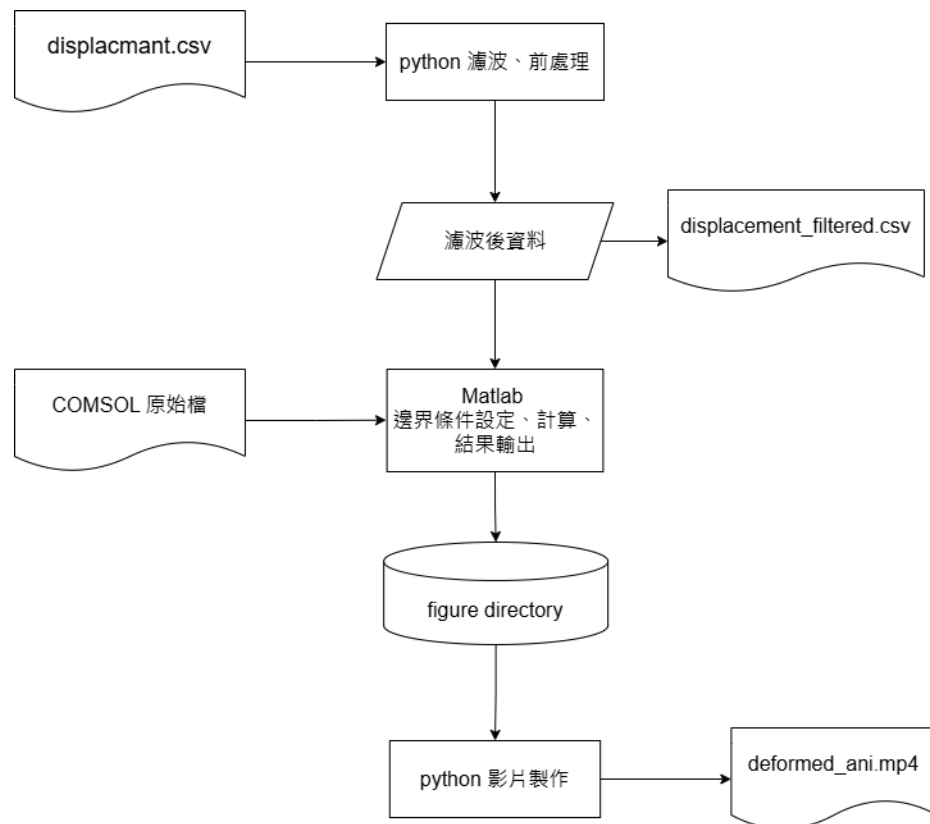


**Figure 29.** COMSOL result output workflow diagram

## 5.6 Deformation Results Visualization

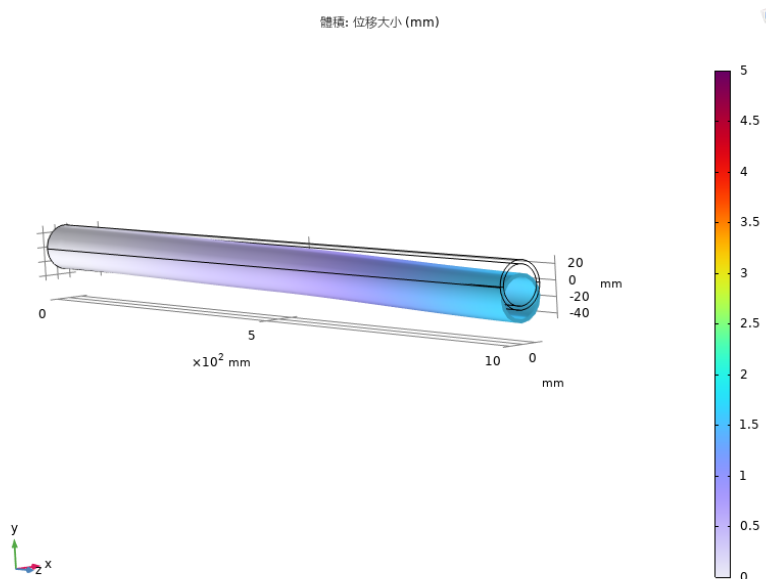


**Figure 30.** Load of 1106 g

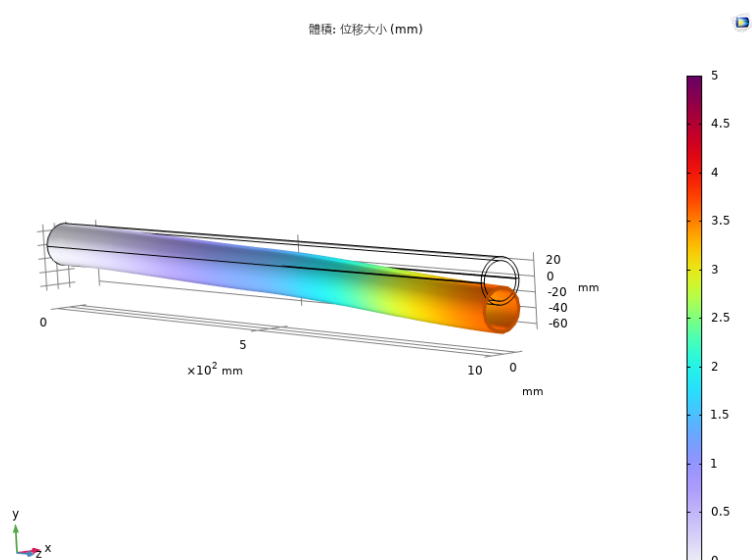


**Figure 31.** Load of 2238.5 g

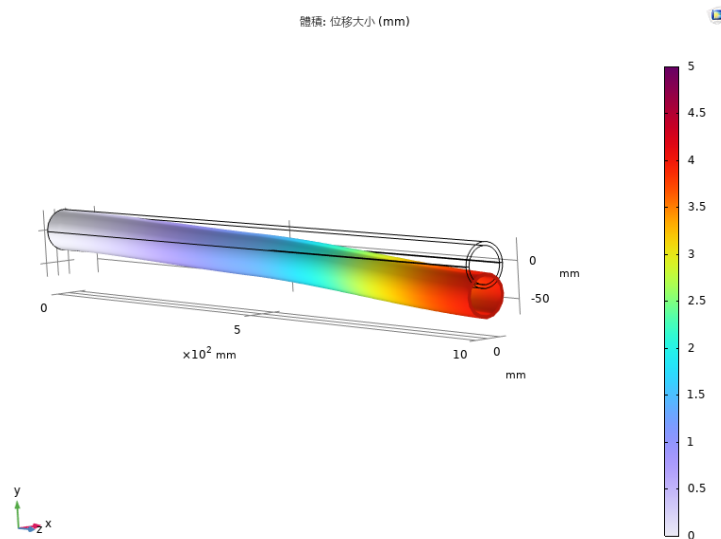


**Figure 32.** Load of 3167 g